Journal of Power Sources 201 (2012) 128–135

Contents lists available at SciVerse ScienceDirect

Journal of Power Sources

journal homepage: www.elsevier.com/locate/jpowsour

Enhanced sulfur and carbon coking tolerance of novel co-doped ceria based anode for solid oxide fuel cells

Xiaoliang Zhou [a,b,c], Jiangman Zhen [c], Limin Liu [c], Xiaokun Li [c], Naiqing Zhang [b,c], Kening Sun [b,c,*]

[a] State Key Laboratory of Urban Water Resource and Environment, Harbin Institute of Technology, Harbin 150090, PR China
[b] Natural Science Research Center, Academy of Fundamental and Interdisciplinary Sciences, Harbin Institute of Technology, Harbin, Heilongjiang 150080, PR China
[c] Department of Applied Chemistry, Harbin Institute of Technology, No. 92 of West Dazhi Street, P.O. Box 211, Harbin, Heilongjiang 150001, PR China

ARTICLE INFO

Article history:
Received 7 October 2011
Received in revised form 27 October 2011
Accepted 31 October 2011
Available online 6 November 2011

Keywords:
Solid oxide fuel cell
Methane
Carbon deposition
Sulfur tolerance
Rare earth elements

ABSTRACT

Doubly doped CeO_2 based anode with Y and Yb is first reported for direct methane solid oxide fuel cells. The power output of the cell with Ni–$Ce_{0.8}Y_{0.1}Yb_{0.1}O_{1.9}$ anode and stability at various temperatures are investigated when air is used as oxidant and pure H_2, 5 ppm H_2S containing H_2 and dry CH_4 as fuel, respectively. At 750 °C, the cell displays stable power output for 120 h at 200 mA cm^{-2} when fueled with dry CH_4, suggesting the carbon deposit is largely absent on the anode, which is confirmed by the SEM observation and EDS results. The results also prove that the rare earth elements Y and Yb affect the sulfur tolerance performance of the anode in a cooperative fashion leading to good anode stability in the contaminated fuel. The SEM and EDS results provide evidence that the cell with Ni–$Ce_{0.8}Y_{0.1}Yb_{0.1}O_{1.9}$ anode is tolerant toward the H_2S contamination. The remarkable performances suggest that co-doped CeO_2 anode is an attractive electrode component for direct hydrocarbon solid oxide fuel cells and might also be used as a catalyst for reforming of hydrocarbon fuels and for removal of fuel gas contaminations such as sulfur.

1. Introduction

Solid oxide fuel cells (SOFCs) represent the cleanest, most efficient and versatile conversion system from chemical energy to electrical energy [1]. The direct electrochemical oxidation of dry hydrocarbon fuels to generate electrical power has the potential to substantially accelerate the use of fuel cells in transportation and distributed-power applications [2–7]. The conventional anode consisting of nickel and yttria-stabilized zirconia (YSZ) has good catalytic activity for fuel oxidation as well as good conductivity for current collection and compatibility with the YSZ electrolyte for easy cell fabrication. However, it is highly susceptible to carbon buildup (coking) and deactivation (poisoning) by contaminants commonly encountered in readily available fuels [8]. Some contaminants (e.g., sulfur impurities) can degrade its performance even at levels of parts per million (ppm) [9]. Therefore, one of the grand challenges is the creation of an anode with high carbon coking and sulfur tolerance ability at intermediate and low temperatures.

In view of these problems, researchers have done substantial work to develop novel anode materials [4,10–17]. Fig. 1 shows the schematic diagram of anode development overview for SOFCs. In regard to anode materials, the anodes with fluorite and perovskite have been the focus of research and development along two main ideas, cermet anode and perovskite anode. Murray et al. reported their pioneering work about the direct electrochemical oxidation of methane using ceria-containing anodes and low operating temperatures to avoid carbon deposition [4]. The use of CeO_2-based anodes demonstrated the potential for direct use of methane. Park et al. developed a composite anode of copper and samaria-doped ceria for the direct electrochemical oxidation of various hydrocarbons [18]. However, the low melting point of Cu makes it difficult to fabricate anode-supported cells using conventional co-firing ceramic methods. In addition the poor catalytic activity of Cu for fuel oxidation restricts cell power output. Zhan and Barnett applied Ru to the conventional Ni–YSZ anode to allow internal hydrocarbons reforming. The introduction of Ru confirmed the direct use of iso-octane without coking in a SOFC [11]. However, the high cost of Ru makes the practical application unlikely.

Considering anode development, the anode with perovskite structure showed different degrees of improved tolerance to carbon coking, and/or sulfur tolerance under various SOFC operating conditions. Tao and Irvine reported a nickel-free SOFC anode $La_{0.75}Sr_{0.25}Cr_{0.5}Mn_{0.5}O_3$ with comparable electrochemical performance to Ni–YSZ cermets and achieved good performance for methane oxidation [10], which was stable in both fuel and air conditions and showed stable electrode performance in methane,

* Corresponding author at: Department of Applied Chemistry, Harbin Institute of Technology, No. 92 of West Dazhi Street, P.O. Box 211, Harbin, Heilongjiang 150001, PR China. Tel.: +86 451 86412153; fax: +86 451 86412153.
E-mail addresses: keningsun@yahoo.com.cn, xlzhou@hit.edu.cn (K. Sun).

0378-7753/$ – see front matter © 2011 Elsevier B.V. All rights reserved.
doi:10.1016/j.jpowsour.2011.10.129

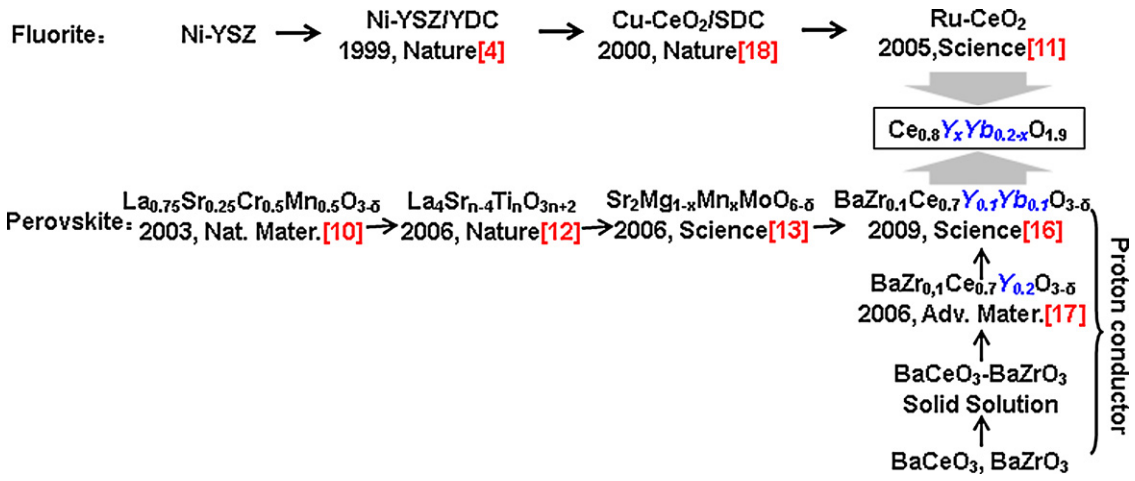

Fig. 1. Schematic diagram of anode development overview for solid oxide fuel cells and present work.

although it has been found to form MnS, La_2O_2S and α-MnOS upon exposure to 10% H_2S [19]. Huang et al. reported the double perovskites $Sr_2Mg_{1-x}Mn_xMoO_{6-\delta}$ met the requirements for long-term stability with tolerance to sulfur and showed excellent single-cell performance in either hydrogen or methane [13]. Acceptable fuel cell performance was found for fuel cells with Sr_2MgMoO_6 or Sr_2MnMoO_6 anodes while using platinum as the current collector, however, in fact platinum is not an inert current collector [21]. In a recent report, it was found that the catalytic activity of $SrMoO_3$ anode is not ideal for SOFC anode [8]. Ruiz-Morales et al. described an oxide anode formed from La–$SrTiO_3$ through controlling the oxygen stoichiometry to break down the extended defect intergrowth regions and create phases with considerable disordered oxygen defects [12]. The material demonstrated impressive fuel cell performance using wet hydrogen at 950 °C and efficient electrode operation with different hydrocarbon fuels [4,22]. However, an initial drop of substantial magnitude in power output when exposing to H_2S contaminated fuels still appeared unavoidable before the mixed ion conductor $BaZr_{0.1}Ce_{0.7}Y_{0.2-x}Yb_xO_{3-\delta}$ was found in 2009 [16]. The development evolution of this material is shown in Fig. 1 [17]. However, to date the mechanism of the anode process is not very clear. The authors believed that the two dopants on the B-site functioned in a cooperative way to improve the ionic conductivity, the catalytic activity and conversion of H_2S to SO_2. Recently, we prepared the $BaZr_{0.1}Ce_{0.7}Y_{0.1}Yb_{0.1}O_{3-\delta}$ powders by ethylene diamine tetraacetic acid assisted glycine nitrate process, finding that the zirconia aggregated in the bulk material [23]. The phase instability was also found in the BaO–ZrO_2–$YO_{1.5}$ system [24]. In this current paper, we report a novel ion conductor, $Ce_{0.8}Y_{0.1}Yb_{0.1}O_{1.9}$, which exhibits higher ion conductivity than the single doped CeO_2 ($Ce_{0.8}Y_{0.2}O_{1.9}$ and $Ce_{0.8}Yb_{0.2}O_{1.9}$) at relatively low temperatures (400–750 °C). Its ability to resist deactivation by sulfur and carbon coking appears linked to the collaborative mechanism of the rare earth elements for sulfur oxidation and hydrocarbon cracking and reforming. We believe that the two rare earth element dopants probably function in a cooperative fashion to improve the ionic conductivity and the catalytic activity for reforming or oxidation of hydrocarbons as well as the conversion of H_2S to SO_2.

2. Experimental details

2.1. Electrode and electrolyte powders preparation

All the powders of the materials $Ce_{0.8}Y_xYb_{0.2-x}O_{1.9}$ (x = 0, 0.1, 0.2) were synthesized by glycine nitrate process (GNP). Stoichiometric amounts of high-purity cerium nitrate, ytterbium oxide and yttrium oxide were dissolved in nitric acid to form a mixed solution under heating and strong stirring. Subsequently, the solution was introduced by glycine. The pH value of the solution used was adjusted to 6–7 by adding further amounts of 1N NH_4OH solution. The mole ratio of total metal ions:glycine was controlled to be 1:1.6. With the evaporation of water, a yellow gel was obtained. After the gel was placed in an oven at 500 °C, the combustion reaction took place within a few seconds, forming the primary powders in light yellow, which were subsequently calcined at 600 °C for 2 h. For the ionic conductivity measurement, the pre-calcined powders were isostatically pressed into a disk at 300 MPa. The disks were then sintered at 1350 °C for 4 h in air to achieve relative density >95%. GDC ($Ce_{0.9}Gd_{0.1}O_{1.95}$) powders used as electrolyte and electrode in this experiment were also synthesized by glycine nitrate process using the corresponding metal nitrates as precursors as well as the identical synthesizing process. The cathode powders $Ce_{0.9}Gd_{0.1}O_{1.95}$ + $La_{0.6}Sr_{0.4}Co_{0.2}Fe_{0.8}O_{3-\delta}$ (GDC + LSCF) were obtained from Fuel Cell Materials Co. (America).

2.2. Fabrication of test cells

The electrolyte-supported button cells with anode Ni–$Ce_{0.8}Y_xYb_{0.2-x}O_{1.9}$ (x = 0, 0.1, 0.2) or Ni–GDC were fabricated as follows. First of all, the as-prepared GDC powders were isostatically pressed into disks with 15 mm in diameter and ~1 mm in thickness, followed by sintering at 1400 °C for 4 h. The sintered ceramic disks were then automatically polished by a machine to become thin and smooth. The thickness was controlled to ~300 μm. Second, a mixture of NiO and $Ce_{0.8}Y_xYb_{0.2-x}O_{1.9}$ powders (weight ratio of 65:35) and LSCF + GDC were made into inks with a binder, cellulose. NiO–$Ce_{0.8}Y_xYb_{0.2-x}O_{1.9}$ was screen-printed to one side of GDC electrolyte with the active electrode areas 0.16 cm^2 and subsequently baked at 1200 °C for 2 h to form a porous anode (~25 μm). The LSCF + GDC cathode was prepared by the same method. The cathode was fired at 1100 °C for 2 h. The cathode layer thickness was about 50 μm. The preparation of the cell with the configuration Ni–YSZ|YSZ|YSZ + LSM has been described in the paper [25]. The active electrode areas for all cells were 0.16 cm^2. Furthermore, the anode exhibits a fine uniform microstructure with an estimated 30% porosity. In this study, $Ce_{0.8}Y_{0.1}Yb_{0.1}O_{1.9}$, Ni–$Ce_{0.8}Y_{0.2}O_{1.9}$ and Ni–$Ce_{0.8}Yb_{0.2}O_{1.9}$ are abbreviated as CYYb, CY and CYb, respectively, for convenience.

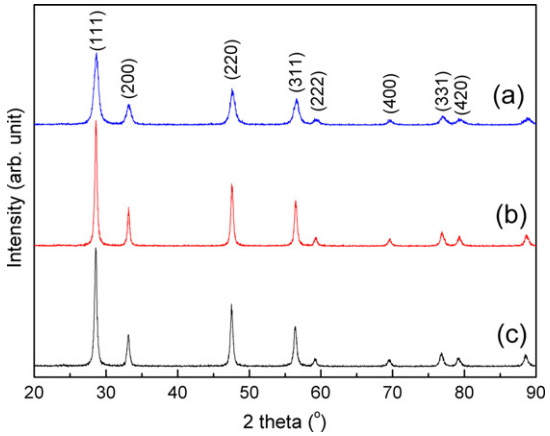

Fig. 2. XRD patterns of $Ce_{0.8}Y_xYb_{0.2-x}O_{1.9}$ (x = 0–0.2) powders. (a) $Ce_{0.8}Y_{0.2}O_{1.9}$; (b) $Ce_{0.8}Y_{0.1}Yb_{0.1}O_{1.9}$; and (c) $Ce_{0.8}Yb_{0.2}O_{1.9}$.

2.3. Power output and electrochemical testing of the cells

For conductivity measurement, Pt paste was coated on the $Ce_{0.8}Y_xYb_{0.2-x}O_{1.9}$ pellet and sintered at 800 °C for 0.5 h to remove the organics, and then Pt electrode was prepared. Ag wire was attached to the Pt electrode. The ionic conductivities of $Ce_{0.8}Y_xYb_{0.2-x}O_{1.9}$ were investigated by AC impedance spectroscopy from 400 to 800 °C using a potentiostat/galvanostat (model PARSTAT* 2273, Princeton Applied Research). The impedance frequency range was 10 mHz to 10 MHz with a signal amplitude of 5 mV. The impedance fitting analysis was controlled with software Zsimpwin.

For H_2S tolerance tests, each button cell was sealed on an alumina tube and heated up to different temperatures ranging from 600 to 750 °C. H_2S concentration was controlled by mixing H_2 and a certified mixture gas containing 100 ppm H_2S in H_2 using two mass flow controllers. The flow rate was 100 ml min^{-1}. All fuel cells were first conditioned at a constant current density in clean H_2 to obtain steady state performance before switching to H_2S-containing H_2. For carbon coking resistance testing in dry CH_4, following reduction of anode in H_2, the cell was conditioned in H_2 as was just described, and then dry CH_4 with a flow rate of 50 mL min^{-1} was fed into the cell at various temperatures. The performance of the cells was performed using Arbin fuel cell testing system.

2.4. Chemical and structural characterization

The phase compositions of the as-synthesized powders were identified by X-ray diffraction (XRD) analysis on Rigaku D/max-2000 X-ray diffractometer with monochromatic Cu Kα radiation (45 kV, 50 mA). The microstructures of the cells after testing were observed using a scanning electron microscope (SEM, HITACHI, S-4700) coupled with INCA energy-dispersive X-ray spectroscopy (EDS). The thermal expansion of the sintered disks of the $Ce_{0.8}Y_xYb_{0.2-x}O_{1.9}$ in air was studied using a NETZSCH DIL 402PC dilatometer. All standard electrochemical experiments were performed using an advanced electrochemical system (model PARSTAT* 2273, Princeton Applied Research).

3. Results and discussion

3.1. X-ray diffraction analysis

To ensure the complete dissolution of dopants in CeO_2, XRD patterns were measured for all the doped ceria samples (sintered at 873 K). Fig. 2 shows XRD patterns of various Yb-doped $Ce_{0.8}Y_{0.2}O_{1.9}$.

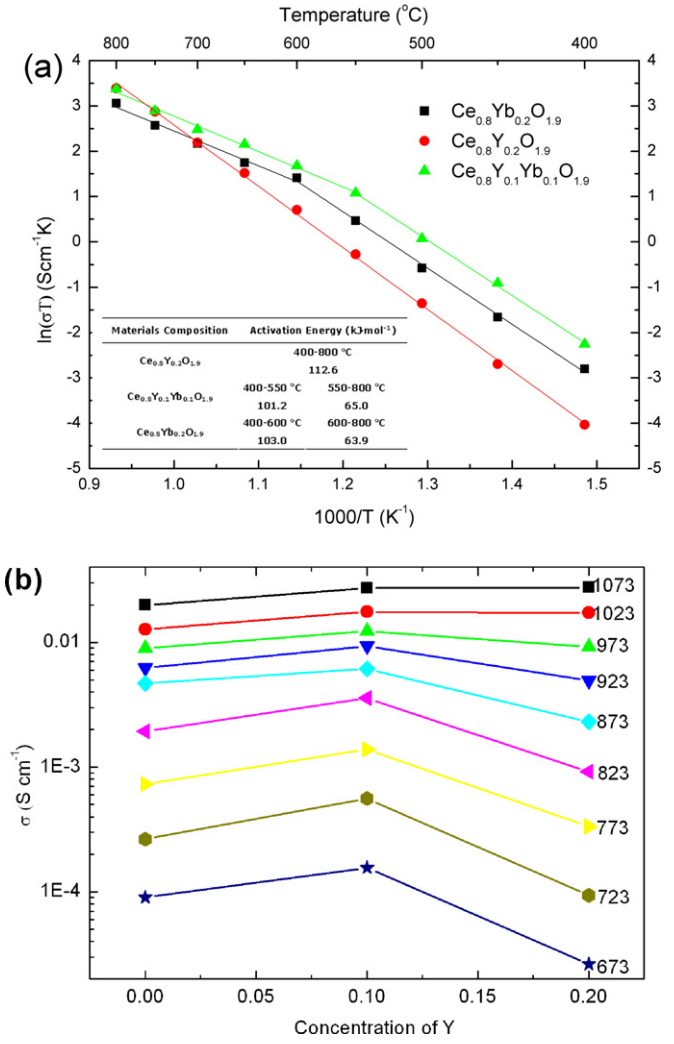

Fig. 3. (a) Arrhenius plots of $Ce_{0.8}Y_xYb_{0.2-x}O_{1.9}$ conductivities as measured at 400–800 °C in air. Inset shows the activation energies of the samples under different temperature ranges and (b) the conductivities of $Ce_{0.8}Y_xYb_{0.2-x}O_{1.9}$ (x = 0–0.2) in air and at different temperatures as a function of the concentration of Y. The number by each set of data represents the absolute temperature at which the conductivity was measured.

It was found that the XRD patterns of the doped ceria samples are different from those of pure Yb_2O_3 and Y_2O_3, but similar to that of pure CeO_2. A pattern for a pure fluorite resembling that of $Ce_{0.8}Sm_{0.2}O_{1.9}$ (SDC) can be observed. It is clear that Yb has replaced Y and has been doped into the lattice of $Ce_{0.8}Y_{0.2}O_{1.9}$ properly. These results indicate that all the doped ceria samples studied are single phase with a cubic fluorite structure. Furthermore, XRD patterns of the materials did not change after high temperature sintering process and conductivity measurements in air, suggesting that the samples are quite stable over a wide range of temperatures.

3.2. Ionic conductivity

In SOFCs, the anode performance was determined largely by the ionic and electrical conductivities of the anode materials. Consequently, the ionic conductivity of $Ce_{0.8}Y_xYb_{0.2-x}O_{1.9}$ in air was investigated after the dense samples were obtained through sintering at 1350 °C for 4 h as confirmed by the relative density measurement and SEM examination. The conductivities of $Ce_{0.8}Y_{0.1}Yb_{0.1}O_{1.9}$ were higher than those of $Ce_{0.8}Y_{0.2}O_{1.9}$ and $Ce_{0.8}Yb_{0.2}O_{1.9}$. Fig. 3(a) shows Arrhenius plots of $Ce_{0.8}Y_xYb_{0.2-x}O_{1.9}$ conductivities measured at 400–800 °C in air. The values of the

activation energy for the ionic conduction under various temperature ranges are shown in the inset. In air, the activation energies for $Ce_{0.8}Y_{0.1}Yb_{0.1}O_{1.9}$ were 101.2 kJ mol^{-1} at 400–550 °C and 65.0 kJ mol^{-1} at 550–800 °C, respectively. It means that there were different activation energies for ionic conduction of $Ce_{0.8}Y_{0.1}Yb_{0.1}O_{1.9}$ in various temperature ranges. Fig. 3(b) shows the conductivities of $Ce_{0.8}Y_xYb_{0.2-x}O_{1.9}$ (x = 0–0.2) in air at different temperatures. The conductivities in air increased quickly with increasing Y concentration, reaching a maximum at 10%. However, with any further increase in the concentration of Y dopant, the conductivities decreased except at the temperatures of 750 and 800 °C. It is interesting to note that ceria containing multiple dopants has a higher conductivity than that containing a single dopant in many cases, which might usher a new method for the design of high-conductivity oxygen ion conductors.

3.3. Thermal expansion behavior

Anode must have a comparable coefficient of thermal expansion (CTE) with the other cell components to minimize thermal stresses because they are running at high temperatures. Fig. 4 shows the thermal expansion curves of pallets $Ce_{0.8}Y_xYb_{0.2-x}O_{1.9}$ (x = 0–0.2) in the temperature range of 30–1400 °C in air. The thermal expansion coefficient data between 100 and 1000 °C were calculated and listed in the inset. It was found that the CTEs of $Ce_{0.8}Y_{0.2}O_{1.9}$, $Ce_{0.8}Y_{0.1}Yb_{0.1}O_{1.9}$ and $Ce_{0.8}Yb_{0.2}O_{1.9}$ were 14.33×10^{-6}, 14.48×10^{-6} and 14.43×10^{-6} K^{-1}, respectively. These values are very comparable to other components of IT-SOFC, such as YSZ electrolyte, Sr-doped $LaFeO_3$ cathode. Therefore, it would be possible to minimize the thermal stress developed during stack start up and shutdown when these materials are used as anode or electrolyte for SOFCs.

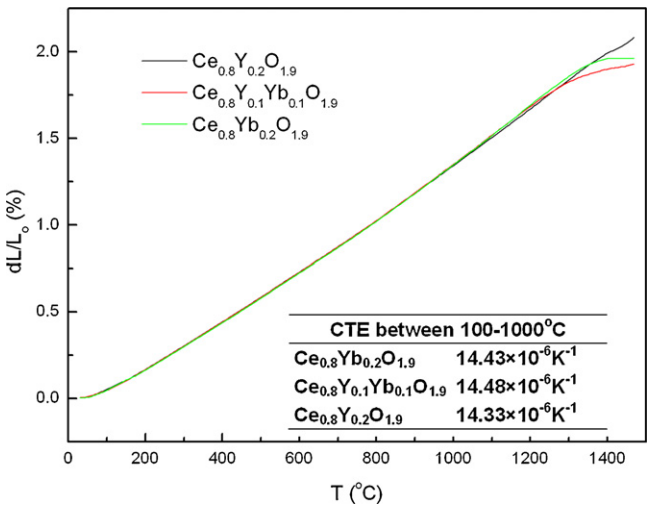

Fig. 4. Thermal expansion curves of pallets $Ce_{0.8}Y_xYb_{0.2-x}O_{1.9}$ (x = 0–0.2) in the temperature range of 30–1400 °C measured in air. Inset shows the values of CTE of the pellets with different compositions between 10 and 1000 °C.

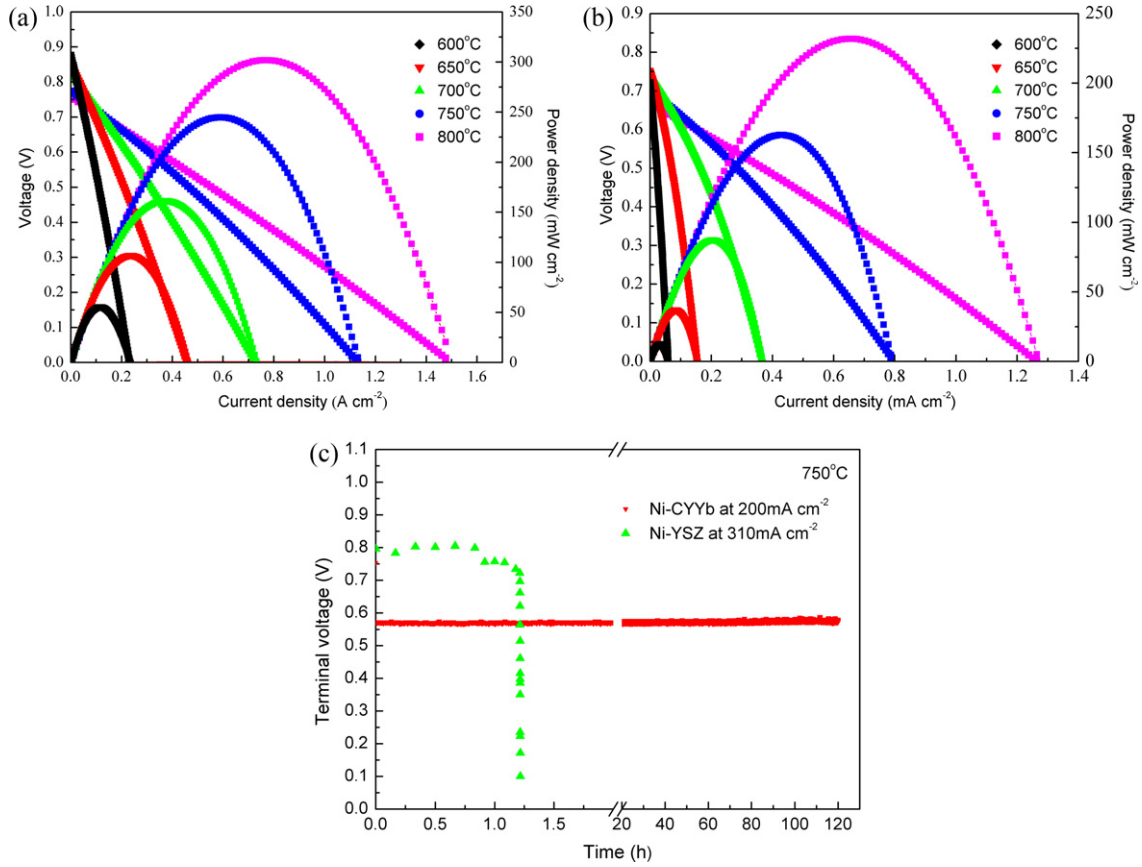

Fig. 5. (a) Typical current–voltage characteristics and the corresponding power densities measured at various temperatures with a configuration of Ni–CYYb|GDC|GDC + LSCF when air was used as oxidant and hydrogen as fuel; (b) typical current–voltage characteristics and the corresponding power densities measured at various temperatures with a configuration of Ni–CYYb|GDC|GDC + LSCF when air was used as oxidant and dry CH_4 as fuel; and (c) terminal voltage measured at 750 °C as a function of time for the cell with Ni–CYYb as the anode operated at a constant current density of 200 mA cm^{-2} with dry CH_4 as the fuel.

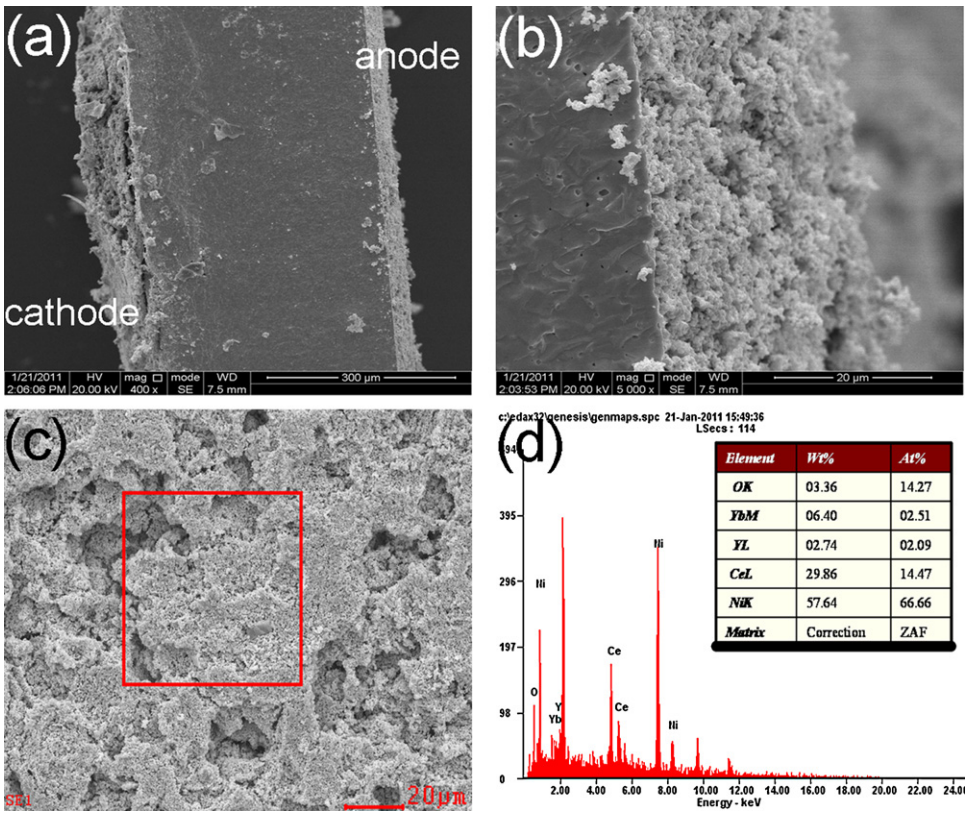

Fig. 6. (a) SEM image of electrolyte-supported SOFC showing the electrolyte layer and electrode layers; (b) magnified fractured cross-sectional SEM image of the Ni–CYYb anode; (c) surface of the Ni–CYYb after testing; and (d) The EDS spectrum of the Ni–CYYb anode surface showing no detectable carbon.

3.4. Power output and durability of fuel cells in dry CH_4

To examine the electro-catalytic activity of the novel anode Ni–CYYb in the electrolyte-supported cells toward the hydrocarbon fuels, we investigated the current–voltage characteristics and measured the corresponding power densities of fuel cells consisting of such an anode, a GDC electrolyte and GDC + LSCF cathode operated with dry CH_4 and the performance in hydrogen was also investigated for comparison. Fig. 5(a) shows the typical current–voltage characteristics and the corresponding power densities at various temperatures when air was used as oxidant and hydrogen as fuel. Due to the occurrence of the electron conduction in the electrolyte GDC at high temperatures, the open circuit voltages of the cells were lower than 1.1 V, and decreased with the increase of the temperature. At 650, 700, 750 and 800 °C, the power densities at 0.6 V were 94, 135, 187 and 202 mW cm^{-2}, respectively. For SOFC, the direct use of hydrocarbon fuel would eliminate a reformer from the system and be beneficial for minimizing the system size as well as improving the system efficiency, resulting in accelerating the commercialization of the SOFC system for a variety of applications. Therefore, we have put our focus on the fuel of CH_4 taking into account its easy availability and low cost. Fig. 5(b) shows the typical current–voltage characteristics and the corresponding power densities measured at various temperatures with a configuration of Ni–CYYb|GDC|GDC + LSCF when air was used as oxidant and dry CH_4 as fuel. At 650, 700, 750 and 800 °C, the power densities at 0.6 V were 30, 64, 83 and 94 mW cm^{-2}, respectively. All the values are lower than those of the cell fueled with H_2 owing to the comparably inert electrode process. Although the performances for these cells in dry CH_4 were not very high owing to the cell configuration, the higher power output would be obtained when the anode-supported cell configuration is adopted. Furthermore, the cell displayed stable power output at 750 °C for 120 h at a constant current density of 200 mA cm^{-2}. After the operation of the cell in dry CH_4 the performance of power output increased by 1.39% instead of performance degradation suggesting that the carbon deposit was largely absent on the anode. For comparison, the conventional Ni–YSZ anode, tested under identical operating conditions, dropped rapidly in dry CH_4, due primarily to carbon buildup and deactivation of the anode (Fig. 5(c)). Subsequent SEM inspection of the fractured cross-section of the cell, the Ni–CYYb anode and the anode surface as shown in Fig. 6(a)–(c) shows that minimal carbon deposition occurred on the novel anode, which was further confirmed by the EDS spectrum. The SEM images provide evidence that the cell with Ni–CYYb anode can increase the

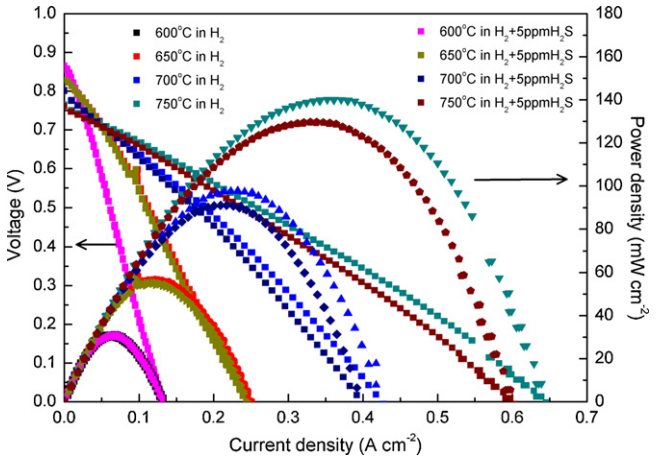

Fig. 7. Typical current–voltage characteristics and the corresponding power densities for the cells with Ni–CYYb anode at different temperatures when H_2 and 5 ppm H_2S containing H_2 were used as the fuel, respectively, and ambient air as the oxidant.

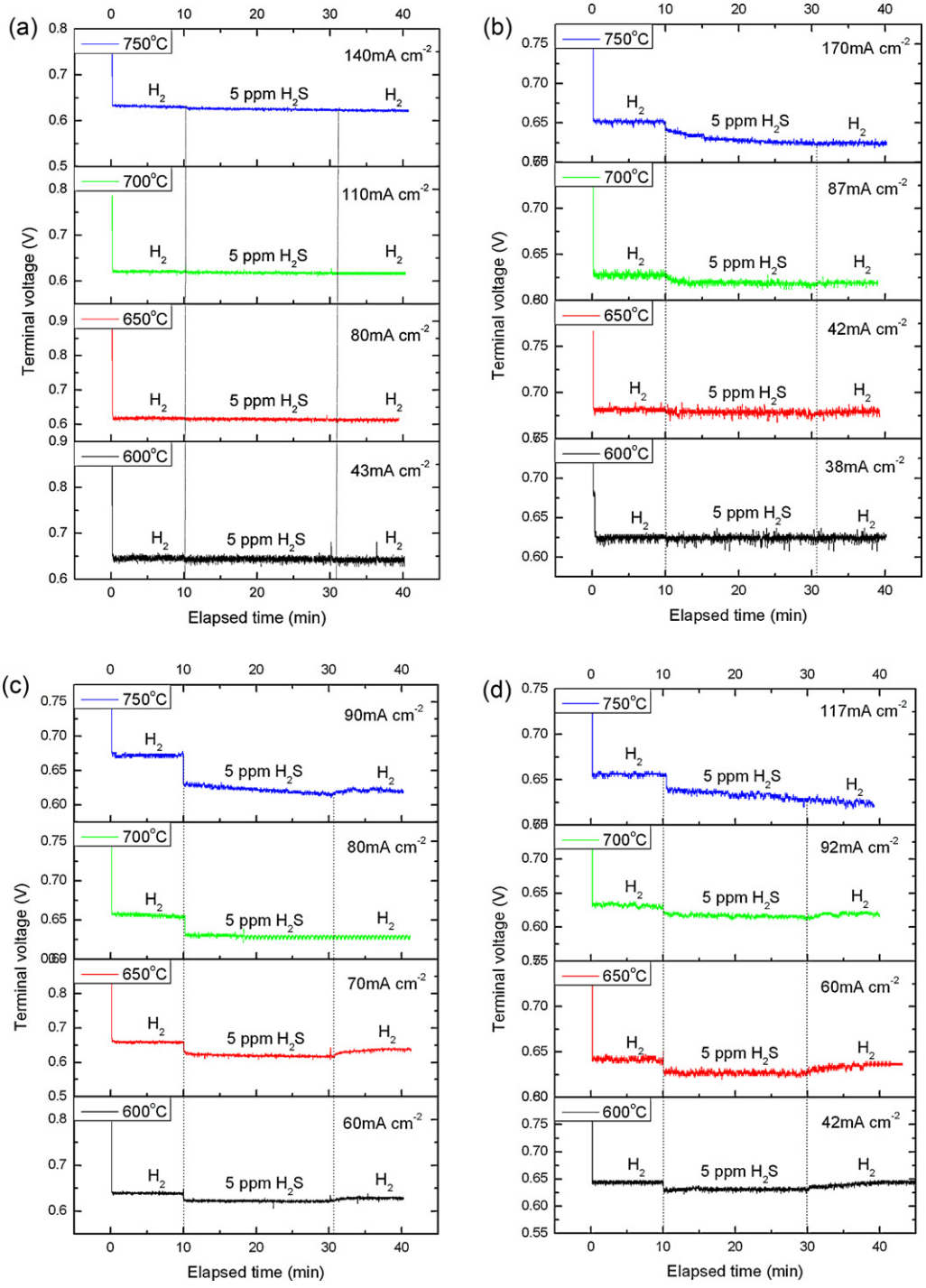

Fig. 8. Terminal voltages measured at different temperatures as a function of time for the cells with different anodes operated at different constant current densities as the fuel switched from clean H_2 to H_2 contaminated with 5 ppm H_2S and then back to clean H_2. (a) Ni–CYYb anode; (b) Ni–CY anode; (c) Ni–CYb anode; and (d) Ni–GDC anode.

cell's tolerance toward the carbon coking and no observable carbon deposits blocking the pores were found. Fig. 6(d) provides evidence that the carbon signal of the Ni–CYYb anode was not significant which indicates that the anode in these experiments did not result in much carbon coking at the surface of the Ni–CYYb anode.

3.5. Power output and stability of fuel cells with Ni–CYYb anode in H_2S containing H_2

In order to investigate the influence of the H_2S addition on this novel anode performance, the power output in H_2 and in 5 ppm containing H_2 at different temperatures was measured. Fig. 7 shows polarization and power density for the cell with Ni–CYYb anode at different temperatures using H_2 and 5 ppm H_2S containing H_2 as the fuel, respectively. Before feeding the 5 ppm H_2S containing H_2 at 100 ml min^{-1} as the fuel, the power densities of the cell at 0.6 V using H_2 as the fuel were 100, 73, 50 and 29 mW cm^{-2} at the temperatures of 750, 700, 650 and 600 °C, respectively. When using the 5 ppm H_2S containing H_2 as the fuel, the power densities of the cell at 0.6 V were 91, 70, 49 and 28 mW cm^{-2} at the temperatures of 750, 700, 650 and 600 °C, respectively. As shown by the values of the power densities at 0.6 V, the addition of the H_2S into

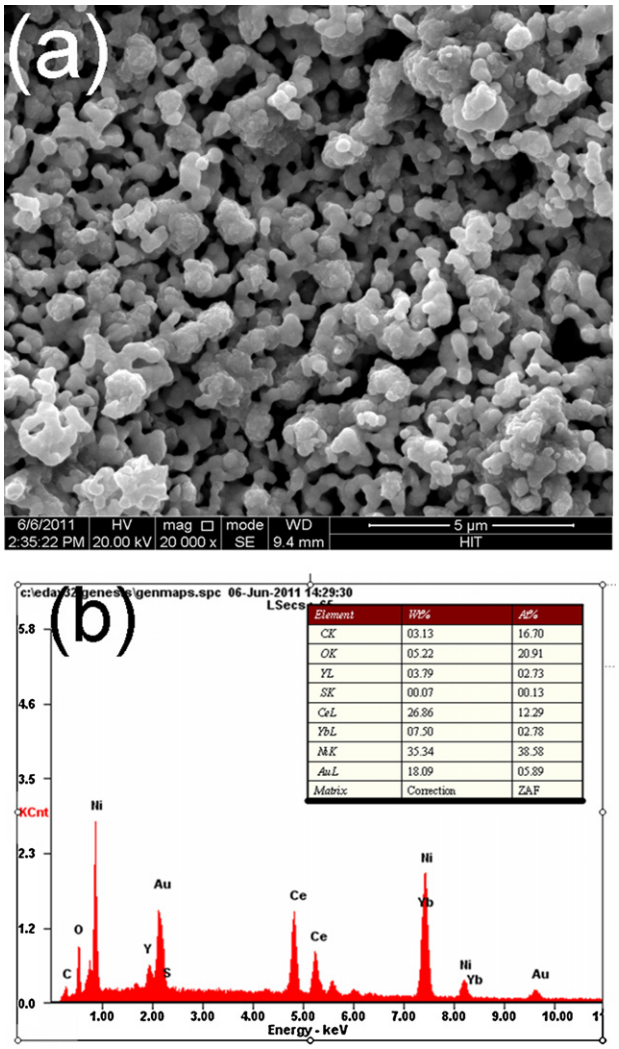

Fig. 9. (a) The 20 K magnification SEM image for the H_2S poisoned cell anode surface of Ni–CYYb and (b) the EDS spectrum of the H_2S poisoned cell anode surface of Ni–CYYb.

the H_2 decreased the performance, indicating that sulfur poisoning had occurred during the operation. At higher temperatures such as 700 and 750 °C, the deactivation of the cell was larger than that at lower temperatures indicating that high temperature accelerated the performance deactivation, and under lower temperature the poisoning effect of the H_2S was alleviated.

It was reported that the novel mixed ion conductor $BaZr_{0.1}Ce_{0.7}Y_{0.2-x}Yb_xO_{3-\delta}$ exhibits high ionic conductivity and the ability to resist deactivation by sulfur and coking results from the two dopants on the B-site functioning in a cooperative fashion to improve the ionic conductivity and the catalytic activity for reforming or oxidation of hydrocarbons as well as conversion of H_2S to SO_2. The good performance of this novel conductor derived from the synergistic effect of the double rare earth elements Y and Yb. In this paper, we studied the synergistic effect of the rare earth elements Y and Yb on the CeO_2 based anode's resistance to sulfur. Fig. 8 shows the terminal voltages measured at different temperatures as a function of time for the cells with different anodes operated at different constant current densities as the fuel switched from clean H_2 to H_2 contaminated with 5 ppm H_2S and then back to clean H_2. As shown in Fig. 8(a), when the fuel was switched to 5 ppm H_2S containing H_2 from the pure H_2, the performance of the cell with Ni–CYYb anode at 750 °C was slightly decreased, and the performance deactivation at higher temperatures was more notable than that at lower temperatures which can be verified by the better performance stability and durability of the cell at 600, 650 and 700 °C, respectively. These results indicated that the power output was not much influenced by the contamination of 5 ppm H_2S consequently exhibiting good stability and durability under the lower temperatures and also indicated that the operation at lower temperatures is in favor of the stable running of the cell. Fig. 8(b)–(d) provides the power output of the cells with the single doped CeO_2 anode, Ni–CY, Ni–CYb and Ni–GDC, respectively. For the cells with single doped CeO_2 anode, the power output marked severe performance decay. Through the comparison the co-doped CeO_2 based anode and single-doped CeO_2 based anode, it can be concluded that the co-dopant rare earth elements Y and Yb affected the sulfur tolerance performance of the anode in a cooperative fashion. Afterwards, the higher durability and stability of the anode against the sulfur poisoning and carbon coking could be obtained by selecting the appropriate co-dopant rare earth elements. The remarkable performances of these cells suggest that co-doped CeO_2 anode is an attractive electrode component for direct hydrocarbon SOFCs. Furthermore, the novel material could also be used as a catalyst for reforming of hydrocarbon fuels and for removal of fuel gas contaminations such as sulfur.

Fig. 9(a) and (b) are the poisoned surface image of the anode and the corresponding EDS results. From the results, it can be seen that after the operation in H_2 contaminated with 5 ppm H_2S, the anode microstructure was still in good condition after H_2S attack. According to the EDS spectrum, the content of element S was 0.13 at.% after the testing, The sulfur signal is not significant which indicates that the exposure of the anode to 5 ppm containing H_2 did not result in much sulfur poisoning. The SEM and EDS results provide evidence that the cell with Ni–CYYb anode is tolerant toward the H_2S contamination.

4. Conclusions

In this paper, the novel materials $Ce_{0.8}Y_xYb_{0.2-x}O_{2-\delta}$ were first reported as the anode for SOFCs. XRD patterns for a pure fluorite resembling that of $Ce_{0.8}Sm_{0.2}O_{1.9}$ were observed. The ionic conductivities of $Ce_{0.8}Y_{0.1}Yb_{0.1}O_{1.9}$ were higher than $Ce_{0.8}Y_{0.2}O_{1.9}$ and $Ce_{0.8}Yb_{0.2}O_{1.9}$. The CTEs of $Ce_{0.8}Y_{0.2}O_{1.9}$, $Ce_{0.8}Y_{0.1}Yb_{0.1}O_{1.9}$ and $Ce_{0.8}Yb_{0.2}O_{1.9}$ were very comparable to other components of SOFCs. The typical current–voltage characteristics and the corresponding power densities at various temperatures with a configuration of Ni–CYYb|GDC|GDC + LSCF were studied when air was used as oxidant and pure H_2, H_2 contaminated with 5 ppm H_2S and dry CH_4 as fuels, respectively. At 650, 700, 750 and 800 °C, the power densities at 0.6 V in dry CH_4 were 30, 64, 83 and 94 mW cm^{-2}, respectively. The cell displayed stable power output at 750 °C for 120 h at a constant current density of 200 mA cm^{-2}, suggesting that the carbon deposit is largely absent on the anode. The carbon signal of the Ni–CYYb anode in the EDS was not significant confirming the anode in these experiments did not result in much carbon coking in the anode. The SEM and EDS results provide evidence that the cell with Ni–CYYb anode is tolerant toward the H_2S contamination leading to good anode stability in 5 ppm containing H_2. The two rare earth element dopants are believed functioning in a cooperative fashion to improve the ionic conductivity and the catalytic activity for reforming or oxidation of hydrocarbons as well as possible conversion of H_2S to SO_2.The above remarkable performances of the cells suggested that co-doped CeO_2 anode is an attractive electrode component for direct hydrocarbon SOFCs. For further study, this novel material might also be used as a catalyst for reforming of hydrocarbon fuels and for removal of fuel gas contaminations such as sulfur. These preliminary results indicate that optimization of the

chemistry and the morphology of these double doped CeO_2 materials can provide an anode material for a SOFC that operates on natural gas or the fuel contaminated with sulfur impurity.

Acknowledgements

This project is financially supported by Natural Science Foundations of China (No. 21106025), Natural Scientific Research Innovation Foundation in Harbin Institute of Technology (No. HIT.NSRIF.2009085), and Open Project of State Key Laboratory of Urban Water Resource and Environment, Harbin Institute of Technology (No. QA201113).

References

[1] R.F. Service, Science 285 (1999) 682.
[2] B.C.H. Steele, A. Heinzel, Nature 414 (2001) 345.
[3] B.C.H. Steele, Nature 400 (1999) 620.
[4] E.P. Murray, T. Tsai, S.A. Barnett, Nature 400 (1999) 649.
[5] E.S. Putna, J. Stubenrauch, J.M. Vohs, R.J. Gorte, Langmuir 11 (1995) 4832.
[6] S. Park, R. Craciun, J.M. Vohs, R.J. Gorte, J. Electrochem. Soc. 146 (1999) 3603.
[7] B.C.H. Steele, I. Kelly, P.H. Middleton, R. Rudkin, Solid State Ionics 28 (1988) 1547.
[8] A. Atkinson, S. Barnett, R.J. Gorte, J.T.S. Irvine, A.J. Mcevoy, M. Mogensen, S.C. Singhal, J. Vohs, Nat. Mater. 3 (2004) 17.
[9] M. Flytzani-Stephanopoulos, M. Sakbodin, Z. Wang, Science 312 (2006) 1508.
[10] S. Tao, J.T.S. Irvine, Nat. Mater. 2 (2003) 320.
[11] Z. Zhan, S.A. Barnett, Science 308 (2005) 844.
[12] J.C. Ruiz-Morales, J. Canales-Vazquez, C. Savaniu, D. Marrero-Lopez, W.Z. Zhou, J.T.S. Irvine, Nature 439 (2006) 568.
[13] Y.H. Huang, R.I. Dass, Z.L. Xing, J.B. Goodenough, Science 312 (2006) 254.
[14] F.Z. Chen, S.W. Zha, J. Dong, M.L. Liu, Solid State Ionics 166 (2004) 269.
[15] O.A. Marina, N.L. Canfield, J.W. Stevenson, Solid State Ionics 149 (2002) 21.
[16] L. Yang, S.Z. Wang, K. Blinn, M.F. Liu, Z. Liu, Z. Cheng, M.L. Liu, Science 326 (2009) 126.
[17] L. Yang, C.D. Zuo, S.Z. Wang, Z. Cheng, M.L. Liu, Adv. Mater. 20 (2008) 3280.
[18] S. Park, J.M. Vohs, R.J. Gorte, Nature 404 (2000) 265.
[19] S. Zha, P. Tsang, Z. Cheng, M. Liu, J. Solid State Chem. 178 (2005) 1844.
[21] B.H. Smith, M.D. Gross, Electrochem. Solid-State Lett. 14 (2011) B1.
[22] S. Primdahl, J.R. Hansen, L. Grahl-Madsen, P.H. Larsen, J. Electrochem. Soc. 148 (2001) A74.
[23] X.L. Zhou, L.M. Liu, J.M. Zhen, S.C. Zhu, B.W. Li, K.N. Sun, P. Wang, J. Power Sources 196 (2011) 5000.
[24] Y. Oyama, A. Kojima, X.Y. Li, R.B. Cervera, K. Tanaka, S. Yamaguchi, Solid State Ionics 197 (2011) 1.
[25] X.L. Zhou, K.N. Sun, J. Gao, S.R. Le, N.Q. Zhang, P. Wang, J. Power Sources 191 (2009) 528.